Doping evolution of the anisotropic upper critical fields in the iron-based superconductor $Ba_{1-x}K_xFe_2As_2$

M. A. Tanatar,[1,2] Yong Liu,[1] J. Jaroszynski,[3] J. S. Brooks,[3,*] T. A. Lograsso,[1,4] and R. Prozorov[1,2]
[1]*Ames Laboratory, U.S. DOE, Ames, Iowa 50011, USA*
[2]*Department of Physics and Astronomy, Iowa State University, Ames, Iowa 50011, USA*
[3]*National High Magnetic Field Laboratory, Florida State University, Tallahassee, Florida 32310, USA*
[4]*Department of Materials Science and Engineering, Iowa State University, Ames, Iowa 50011, USA*
(Received 21 August 2017; revised manuscript received 19 October 2017; published 14 November 2017)

In-plane resistivity measurements as a function of temperature and magnetic field up to 35 T with precise orientation within the crystallographic *ac* plane were used to study the upper critical field H_{c2} of the hole-doped iron-based superconductor $Ba_{1-x}K_xFe_2As_2$. Compositions of the samples studied spanned from underdoped $x = 0.17$ ($T_c = 12$ K) and $x = 0.22$ ($T_c = 20$ K), both in the coexistence range of stripe magnetism and superconductivity, through optimal doping $x = 0.39$ ($T_c = 38.4$ K) and $x = 0.47$ ($T_c = 37.2$ K), to overdoped $x = 0.65$ ($T_c = 22$ K) and $x = 0.83$ ($T_c = 10$ K). We find notable doping asymmetry of the shapes of the anisotropic $H_{c2}(T)$, suggesting the important role of paramagnetic limiting effects in the $H \parallel a$ configuration in overdoped compositions and multiband effects in underdoped compositions.

DOI: 10.1103/PhysRevB.96.184511

I. INTRODUCTION

Distinctive features of the iron-based high-transition-temperature, T_c, superconductors [1] are very high values of the upper critical fields H_{c2} [2] and their low anisotropy with respect to the Fe-As layer (tetragonal or orthorhombic *ab* plane), $\gamma_H = H_{c2}^{ab}/H_{c2}^{c}$ [3–6]. Anisotropy of the upper critical field in the orbital limiting scenario [7] is determined by the anisotropy of the Fermi velocity and thus is linked with resistivity anisotropy $\gamma_\rho \equiv \rho_c/\rho_a$ with $\gamma_\rho \approx \gamma_H^2$ at T_c [8,9]. In uniaxial (tetragonal and hexagonal) crystals, the dependence of the orbital H_{c2} on angle θ with respect to the *ab* plane can be written as

$$H_{c2}(\theta) = \frac{H_{c2}^{ab}}{\sqrt{\left(\gamma_H^2 - 1\right)\sin^2\theta + 1}}. \quad (1)$$

Notable deviations from this angular dependence were found in electron overdoped $Ba(Fe_{1-x}Ni_x)_2As_2$ and discussed in the multiband scenario [10]. Deviations can be particularly pronounced when magnetic field is aligned parallel to the conducting plane, so that orbital upper critical fields can become higher than paramagnetic limit [11]. Crossover between the orbital and paramagnetic limiting mechanisms leads to a difference in the shape of the $H_{c2}(T)$ line, which was noted in KFe_2As_2 [9,12] and nearby hole-overdoped $Ba_{1-x}K_xFe_2As_2$ compositions [13,14]. The importance of the paramagnetic limiting effects was also suggested by the observation of the first-order transition at the $H_{c2}^{ab}(T)$ line at low temperatures in the thermal expansion and magnetostriction measurements in KFe_2As_2 [15], small angle neutron scattering [16] and anomalous hysteresis in field-sweep resistivity measurements [13]. Since close to T_c H_{c2} is always determined by orbital mechanism, one needs to study low temperatures regime where superconducting gap is fully developed. Thus far low-temperature measurements in the underdoped $Ba_{1-x}K_xFe_2As_2$ compositions have been performed only in the $H \parallel c$ configuration [17]. To the best of our knowledge there have been no studies of the anisotropy of H_{c2} in the conducting plane of any of the iron-based superconductors, which is usually neglected as being small compared to *ac*-plane anisotropy, in line with experimental studies in some compounds [18–20].

In hole-doped materials $Ba_{1-x}K_xFe_2As_2$ the slope of the $H_{c2}^{c}(T)$ curves close to zero-field T_c over a broad composition range, $0.22 \leqslant x \leqslant 1$, scales well with T_c, while the γ_H anisotropy somewhat increases for $x > 0.83$ close to $x = 1$ [9,21]. Interestingly, this is the composition range where the superconducting gap also becomes nodal [22–28]. In the end hole-doped composition KFe_2As_2, the upper critical field H_{c2}^{c} strongly changes upon pressure-induced transition [29] between two different superconducting states [30–32]. It was argued that the transformation is consistent with the transformation of the superconducting gap structure, namely, development of horizontal nodes in the superconducting gap [29].

The dependence of the upper critical field on the superconducting gap structure, on proximity to magnetism, and on the topology of the Fermi surface makes doping evolution of the upper critical field in hole-doped $Ba_{1-x}K_xFe_2As_2$ nontrivial. The superconducting state of $Ba_{1-x}K_xFe_2As_2$ (see the doping phase diagram in the bottom panel of Fig. 1) has ranges of coexistence with two different types of magnetism (stripe antiferromagnetic C_2 phase [33] and tetragonal antiferromagnetic C_4 phase [34–36]). The anisotropy of the superconducting gap notably increases in the C_2AF-superconductivity coexistence range [17,37], similar to overdoped compositions. In addition Fermi surface topology changes at $x \sim 0.5$ [38,39] and $x \sim 0.7$–0.8 [40], with the latter also being accompanied by the superconducting gap anisotropy change [26,28].

In this paper we report a comparative study of the precision-alignment anisotropic $H_{c2}(T)$ for underdoped and overdoped compositions of hole-doped $Ba_{1-x}K_xFe_2As_2$ using dc magnetic field up to 35 T in the National High Magnetic Field Laboratory in Tallahassee. The compositions were selected with close values of T_c in the 10 K range ($x = 0.17$, $T_c = 12$ K and $x = 0.83$, $T_c = 10$ K), in the 20 K range

*Deceased.

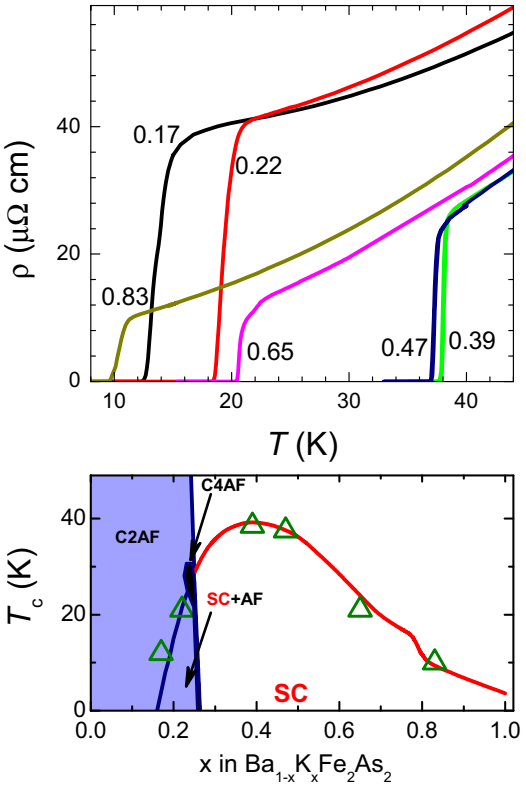

FIG. 1. Top: Temperature-dependent electrical resistivity of selected representative samples of $Ba_{1-x}K_xFe_2As_2$ with $x = 0.17$, 0.22, 0.39, 0.47, 0.65, and 0.83. Compositions were chosen to have T_c of about 10 K on the overdoped ($x = 0.83$) and underdoped ($x = 0.17$) sides, 20 K ($x = 0.65$ and 0.22), and above 35 K ($x = 0.39$ and 0.47). Bottom: Doping phase diagram with the position of the samples studied. C2AF corresponds to a range of the stripe antiferromagnet phase, C4AF corresponds to a range of the tetragonal C_4 antiferromagnetic phase, C4PM corresponds to the tetragonal paramagnetic state, and SC is the domain of the superconductivity, including ranges of coexistence with C2AF and C4AF phases (SC+AF).

($x = 0.22$, $T_c = 20$ K and $x = 0.65$, $T_c = 22$ K), and in the 38 K range close to optimal doping ($x = 0.39$, $T_c = 38.4$ K and $x = 0.47$, $T_c = 37.2$ K). The whole $H-T$ phase diagram could be explored in the 10 K class samples, a large part of it could be explored in the 20 K class samples, and only a small range could be explored in the optimally doped samples. Our main findings are a clear tendency for paramagnetic limiting effects on the overdoped side of the phase diagram and a notable difference in the shape of $H_{c2}^{ab}(T)$ lines in samples of similar T_c in the overdoped and underdoped ranges.

II. EXPERIMENT

Single crystals of $Ba_{1-x}K_xFe_2As_2$ were grown using the self-flux method [21,41]. Samples used for four-probe electrical resistivity measurements were cleaved from the inner parts of large single crystals (with a surface area up to 1 cm^2 and 0.3 mm thickness) and had dimensions of typically (2–3) × 0.5 × 0.1 mm^3, with the longer side along the [100] tetragonal direction. Silver wires were soldered using Sn to the fresh-cleaved surface of the samples [42,43] to make electrical contacts with several microOhm resistance. Sample resistivity at room temperature, $\rho(300\ \mathrm{K})$, was doping independent within statistical error bars of geometric factor determination, ±10%. For all samples it was set to an average value as determined on a big array of crystals, $\rho(300\ \mathrm{K}) = 300\ \mu\Omega$ cm, [8]. Temperature-dependent electrical resistivity $\rho(T)$ measurements were performed down to 1.8 K in a *Quantum Design* physical property measurement system (PPMS) for sample screening. Measurements were performed in zero magnetic field. The sharpness of the zero-field resistive transition was used as a criterion for sample selection. The composition of the selected samples was determined using electron probe microanalysis with wavelength dispersive spectroscopy. In Fig. 1 we show the low-temperature part of temperature-dependent resistivity of selected samples. Their positions on the doping phase diagram are indicated with triangles in the bottom panel of Fig. 1.

Selected samples were glued with GE varnish to a plastic platform, fitting the single-axis rotator of the 35-T dc magnet in the National High Magnetic Field Laboratory. Sample resistance was checked after mounting and was found to be identical to the initial value. The sample's long axis (current direction) was aligned by eye parallel to the rotation axis (with accuracy of about 5°). High-field measurements were made in a He cryostat with a variable-temperature control insert allowing for temperatures down to 1.5 K. The stepping-motor-driven rotator enabled *in situ* rotation with ∼0.1° resolution around a horizontal axis in a single-axis rotation system of vertical 35-T magnetic field. In an ideal case of perfect parallel alignment of sample and rotation axes, during this rotation the direction of the magnetic field with respect to the crystal traverses in the tetragonal (100) plane (ac plane), always remaining perpendicular to the current. However, the field-rotation plane may be somewhat inclined from the (100) plane due to potential misalignment of sample and rotator axes (see [10] for details). This misalignment does not affect precision alignment in the $H \parallel ab$ plane configuration ($\theta = 0$), which was achieved by measuring angle-dependent resistivity in a field slightly below the end of the resistive transition in field close to parallel to the plane configuration (see the inset in the top left panel of Fig. 2).

III. RESULTS

In Fig. 2 we show isothermal magnetic-field sweep resistivity data $\rho(H)$ taken at different temperatures in magnetic fields aligned along the c axis ($\theta = 90°$, top panel) and precisely along the conducting plane ($\theta = 0°$, middle panel) for the underdoped composition of $Ba_{1-x}K_xFe_2As_2$ with $x = 0.17$ (left column of panels). The inset in the top left panel shows angle-dependent resistivity in magnetic field slightly below H_{c2}^{a} used for field alignment parallel to the conducting plane. The bottom left panel summarizes $H-T$ phase diagrams as determined using the transition midpoint criterion (symbols in top and middle panels). The use of this criterion is justified by the small variation of the resistive transition width on application of magnetic field and its independence of the extrapolation, a typical problem for onset and offset criteria. The low value of $T_c = 12$ K in the sample enables complete suppression of superconductivity at the base temperature in

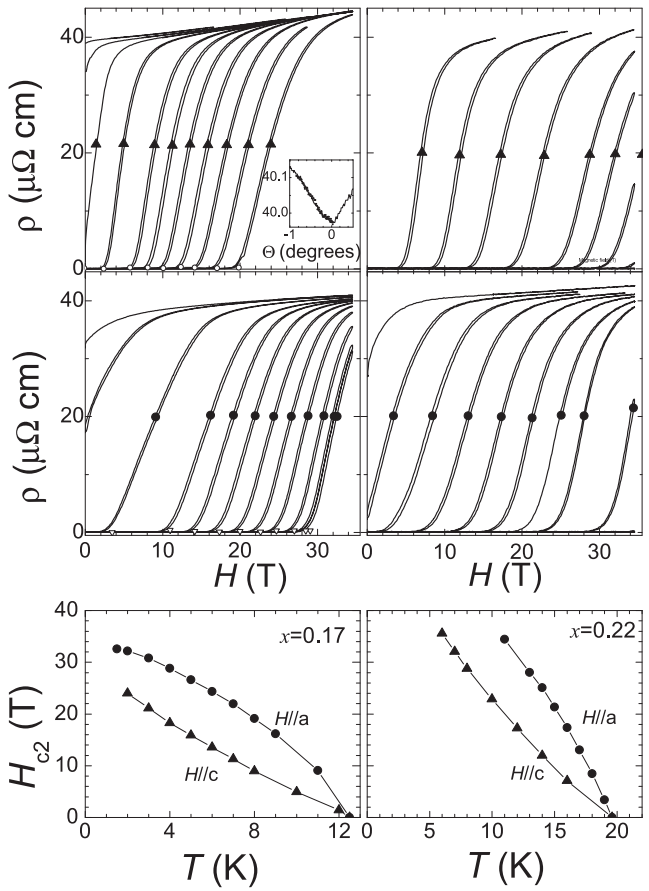

FIG. 2. Left: Magnetic-field-dependent resistivity of underdoped sample $Ba_{1-x}K_xFe_2As_2$, $x = 0.17$, taken in isothermal conditions in magnetic fields oriented along the tetragonal c axis ($H \parallel c$, top panel, temperatures: 16, 14, 12, 10, 8, 7, 6, 5, 4, 3, and 2 K, from left to right) and perpendicular to it ($H \parallel a$, middle panel, temperatures, from left to right: 15, 13, 11, 9, 8, 7, 6, 5, 4, 3, 2, and 1.8 K). The bottom panel shows $H-T$ phase diagrams for two field orientations determined using the midpoint criterion between up- and down-field sweeps. The inset in the top panel shows the sample alignment procedure. Resistivity measurements were taken in field H slightly lower than H^a_{c2}, in which sample resistance shows strong angular dependence. The curve was measured in the one-direction motion of the rotator to avoid backlash, with the deep minimum corresponding to $H \parallel ab$. Right: Magnetic-field-dependent resistivity of underdoped sample $Ba_{1-x}K_xFe_2As_2$, $x = 0.22$, taken in isothermal conditions in magnetic fields oriented along the tetragonal c axis ($H \parallel c$, top panel, temperatures: 16, 14, 12, 10, 8, 7, and 6 K, from left to right) and perpendicular to it ($H \parallel a$, middle panel, temperatures, from left to right: 20, 18, 17, 16, 15, 14, 13, and 11 K). The bottom panel shows $H-T$ phase diagrams for two field orientations determined using the midpoint criterion between up- and down-field sweeps.

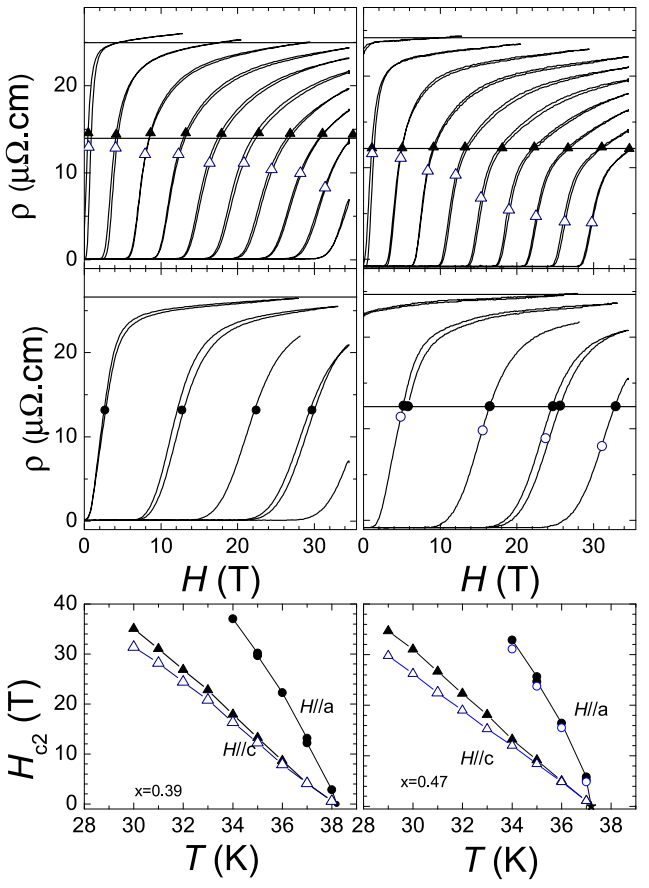

FIG. 3. Left: Magnetic-field-dependent resistivity of sample $Ba_{1-x}K_xFe_2As_2$, $x = 0.39$, taken in isothermal conditions in magnetic fields oriented along the tetragonal c axis ($H \parallel c$, top panel, temperatures: 38, 37, 36, 35, 34, 33, 32, 31, 30, and 29 K left to right), and perpendicular to it ($H \parallel a$, middle panel, temperatures, from left to right: 38, 37, 36, 35, and 34 K). The bottom panel shows $H-T$ phase diagrams for two field orientations determined using the midpoint criterion between up- and down-field sweeps (open symbols) and constant resistance criterion (line and solid symbols). Right: Magnetic-field-dependent resistivity of sample $Ba_{1-x}K_xFe_2As_2$, $x = 0.47$, taken in isothermal conditions in magnetic fields oriented along the tetragonal c axis ($H \parallel c$, top panel, temperatures: 38, 37, 36, 35, 34, 33, 32, 31, 30, and 29 K, from left to right) and perpendicular to it ($H \parallel a$, middle panel, temperatures, from left to right: 38, 37, 36, 35, and 34 K). The bottom panel shows $H-T$ phase diagrams for two field orientations determined using the midpoint criterion between up- and down-field sweeps (open symbols) and constant resistance criterion (lines and solid symbols).

the $H \parallel c$ configuration and essential suppression in the $H \parallel a$ configuration. The data in the $H \parallel c$ configuration are in reasonable agreement with previous measurements in a smaller field-temperature range [17], finding nearly T-linear $H^c_{c2}(T)$ with small up-ward curvature without any sign of saturation on $T \to 0$, contrary to Werthamer-Helfand-Hohenberg (WHH) theory expectations [7]. A clear down-ward curvature with the tendency for saturation is found in the $H^a_{c2}(T)$ curve.

In the top and middle panels of the right column in Fig. 2 we show raw resistivity field-sweep data in a sample with $x = 0.22$; the phase diagram is presented in the bottom panel. Magnetic field of 35 T $H \parallel c$ is sufficient to suppress superconductivity down to $T = 6$ K ($T/T_c \approx 0.3$), while in $H \parallel a$ superconductivity can be suppressed only down to 10 K ($T/T_c \approx 0.5$). Despite a limited range of magnetic field, the temperature-dependent anisotropic $H_{c2}(T)$ reveal the same trend as found in the $x = 0.17$ sample, with close to linear dependence and small up-ward curvatue in $H \parallel c$ and a tendency for saturation in $H \parallel a$.

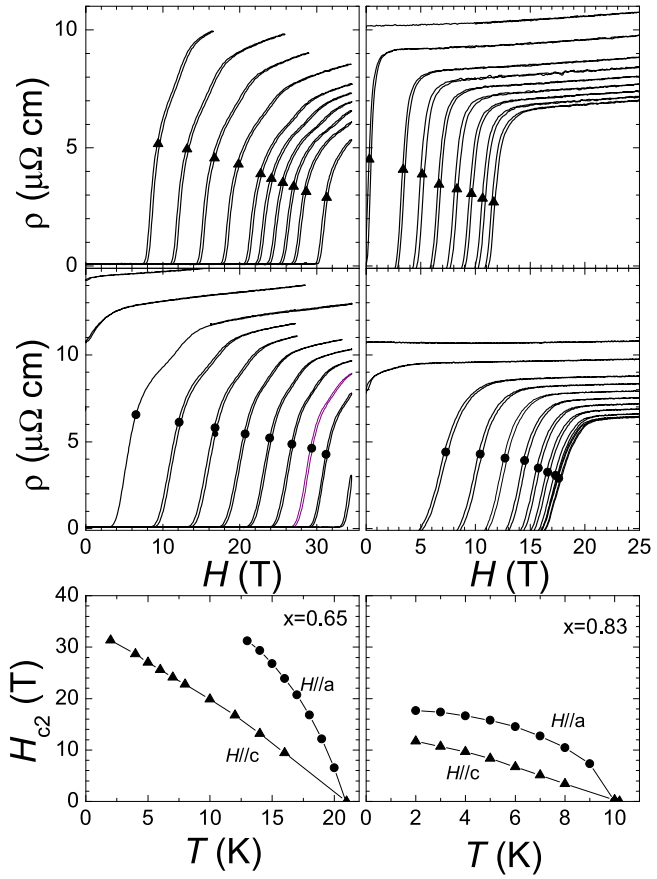

FIG. 4. Left: Magnetic-field-dependent resistivity of sample $Ba_{1-x}K_xFe_2As_2$, $x = 0.65$, taken in isothermal conditions in magnetic fields oriented along the tetragonal c axis ($H \parallel c$, top panel, temperatures: 16, 14, 12, 10, 8, 7, 6, 5, 4, and 2 K, from left to right) and parallel to the plane ($H \parallel a$, middle panel, temperatures, from left to right: 24, 22, 20, 19, 18, 17, 16, 15, 14, 13, and 11 K). The bottom panel shows $H-T$ phase diagrams for two field orientations determined using the midpoint criterion between up- and down-field sweeps. Right: Magnetic-field-dependent resistivity of sample $Ba_{1-x}K_xFe_2As_2$ $x = 0.83$ taken in isothermal conditions in magnetic fields oriented along the tetragonal c axis ($H \parallel c$, top panel, temperatures: 12, 10, 8, 6, 5, 4, 3, and 2 K, from left to right) and perpendicular to it ($H \parallel a$, middle panel, temperatures, from left to right: 11, 9, 8, 7, 6, 5, 4, 3, and 2 K). The bottom panel shows $H-T$ phase diagrams for two field orientations determined using the midpoint criterion between up- and down-field sweeps.

In Fig. 3 we show raw resistivity data (top panels in $H \parallel c$ configurations and middle panels in $H \parallel a$ configurations) and $H-T$ phase diagrams (bottom panels) in samples close to optimal doping, $x = 0.39$ (left column) and $x = 0.47$ (right column). A very narrow part of the phase diagram can be explored with a 35-T magnetic field; however, even in this limited range the difference between close to T-linear H_{c2}^c and down-curving H_{c2}^a is visible. Note the strong variation of the normal-state resistivity with temperature in both samples, which makes determination of H_{c2} using the same resistivity criterion impossible. The transition midpoint is also an ill-defined criterion for the sample because of rounding of $\rho(H)$ curves in the normal state, presumably due to filamentary superconductivity in the normal state.

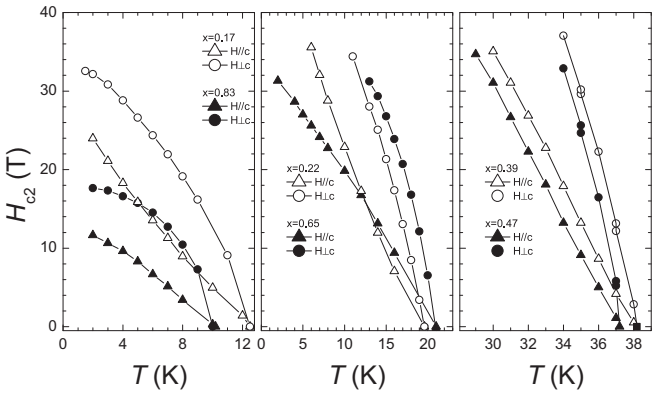

FIG. 5. Left: Comparison of the $H-T$ phase diagrams of a 10 K pair of underdoped ($x = 0.17$) and overdoped ($x = 0.83$) samples. Middle: A similar comparison for a 20 K pair of underdoped ($x = 0.22$) and overdoped ($x = 0.65$) samples. Right: Data for samples close to optimum doping, $x = 0.39$ and $x = 0.47$. Note the clear tendency to saturation in both overdoped compositions for the magnetic-field configuration $H \parallel a$.

In Fig. 4 we show resistivity vs field curves in $H \parallel c$ (top panels) and $H \parallel a$ (middle panels) configurations for overdoped samples $x = 0.65$ (left column) and $x = 0.83$ (right column). A smaller value of T_c enables characterization of the whole phase diagram for the 10 K class sample $x = 0.83$. Note the decrease of the normal-state resistivity on cooling in both compositions, the tendency for $H_{c2}^c(T)$ saturation on cooling, and the pronounced tendency for saturation at temperatures close to zero-field T_c in the $H \parallel a$ configuration.

Experimental summary

In Fig. 5 we make a direct comparison of the $H-T$ phase diagrams of 10 K class samples (underdoped $x = 0.17$ and overdoped $x = 0.83$; left panel), 20 K class samples (underdoped $x = 0.22$ and overdoped $x = 0.65$; middle panel), and optimally doped 38 K samples ($x = 0.39$ and $x = 0.47$; right panel). This comparison highlights the difference between two doping regimes. $H_{c2}^c(T)$ shows a small upward curvature in underdoped compositions, somewhat reminiscent of the dependence in layered superconductors [44] and in multiband superconductors [45]. A slight tendency for saturation of $H_{c2}^c(T)$ may be found in overdoped compositions. A tendency for $H_{c2}(T)$ saturation for orbital limiting is expected to become visible below $T/T_c < 0.3$ [7] (see Fig. 7 below). Deviation from this prediction in iron-based superconductors was discussed in the multiband scenario [10,45]. Indeed, heat-capacity [46] and London penetration-depth studies [28] suggest pronounced multiband effects, with the gap magnitude on different sheets of the Fermi surface varying by a factor of approximately 2.

The dependence in the configuration with magnetic field parallel to the plane is even more intriguing. In Fig. 6 we compare the data for all compositions in precision-aligned $H \parallel a$ conditions. Note the much more pronounced curvature of $H_{c2}^a(T)$ close to zero-field T_c in the overdoped compositions.

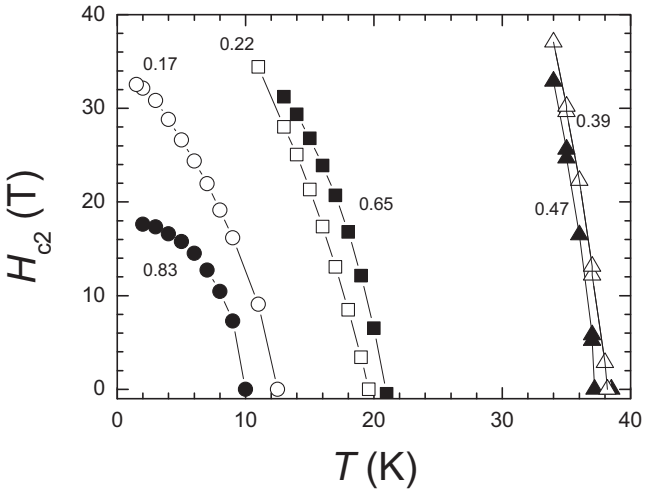

FIG. 6. Comparison of the $H-T$ phase diagrams in parallel magnetic field $H^a_{c2}(T)$ for samples of $Ba_{1-x}K_xFe_2As_2$ for compositions (from left to right) with $x = 0.83$ (solid circles), $x = 0.17$ (open circles), $x = 0.22$ (open squares), $x = 0.65$ (solid squares), $x = 0.39$ (open triangles), and $x = 0.47$ (solid triangles).

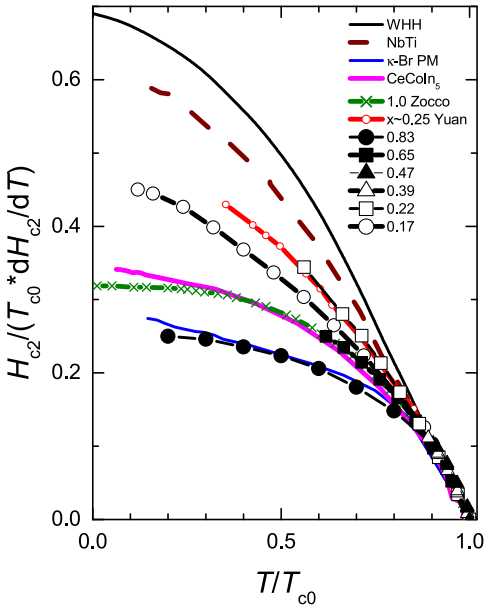

FIG. 7. Comparison of the $H-T$ phase diagrams of $Ba_{1-x}K_xFe_2As_2$ in magnetic field precisely parallel to the plane $H^a_{c2}(T)$ using normalized temperature, T/T_{c0}, and magnetic-field, $H/[T_{c0}dH_{c2}(T)/dT]$, scales. For reference we show expectations for the orbital limiting mechanism in WHH theory [7] (black solid line), the experimentally determined H_{c2} line for the conventional isotropic superconductor NbTi with dominant orbital limiting (dashed brown line), the layered organic superconductor κ-(BEDT-TTF)$_2$Cu[N(CN)$_2$]Br (κ-Br) in magnetic field parallel to the conducting plane in which paramagnetic limiting starts in the close vicinity of T_c [50] (blue line), and paramagnetically limited $CeCoIn_5$ [51] (magenta line). We also plot data for KFe_2As_2 as determined from magnetostriction and thermal expansion measurements in $x = 1$ by Zocco *et al.* [15] (green crosses and line) and from resistivity measurements in pulsed field for a sample with $T_c \approx 28$ K corresponding roughly to $x = 0.25$ from Yuan *et al.* (red line with open circles) [5]. Solid symbols represent overdoped compositions with $x = 0.83$ (circles), $x = 0.65$ (squares), and $x = 0.47$ (triangles). Open symbols are used for underdoped compositions with $x = 0.17$ (circles) and $x = 0.22$ (squares) and for optimally doped $x = 0.39$ (triangles).

IV. DISCUSSION

There are two mechanisms that determine the upper critical field of superconductors. The first one, determined by the supercurrent flow to screen the magnetic field, is referred to as orbital limiting and described by WHH theory [7]. The upper critical field at the $T \to 0$ limit $H_{c2}(0)$ in WHH theory is determined by the slope of the $H_{c2}(T)$ curve close to T_c, and as T goes to zero, the curve shows downward deviation from linear dependence and eventual saturation towards the value $H_{c2}(0) \approx 0.7T_c\frac{dH_{c2}}{dT}$ in the isotropic case. In Fig. 7 we show the temperature-dependent $H_{c2}(T)$ as expected in WHH theory and the data for isotropic NbTi as a typical experimental observation.

Rather rare exceptions, when the upper critical field is not determined by the orbital limiting, are found in the materials in which the orbital motion of electrons is hampered by either a short mean free path, heavy mass of conduction electrons in heavy-fermion materials, or weak links between the conducting layers in Josephson structures or in naturally highly electronically anisotropic layered materials [47,48], provided that the magnetic field is aligned precisely parallel to the conducting layer. In this situation the upper critical field H_{c2} is determined by Zeeman splitting of electron levels, known as the Clogston-Chandrasekhar [11] paramagnetic limit. This field is determined by a decrease of paramagnetic energy, becoming equal to the condensation energy of the superconductor. In weak-coupling BCS superconductors the paramagnetic limiting field is determined in the $T \to 0$ limit as $H_p = 1.8T_c$, where H_p is the field in Teslas and T_c is in Kelvins. Note, however, that even in materials with dominant paramagnetic effects, the behavior of the $H_{c2}(T)$ line close to zero-field T_c is always determined by the orbital limiting mechanism, so that the slope of H_{c2} lines at T_c reflects the anisotropy of the electronic structure. The width of the temperature range in which the orbital limiting mechanism is dominant depends on the ratio of orbital and paramagnetic limiting fields (the Maki parameter) [49]. In strongly anisotropic materials, like organic κ-(BEDT-TTF)$_2$Cu[N(CN)$_2$] Br ($T_c = 12.8$ K, $\gamma_\rho \sim 10^4$), where BEDT-TTF stands for bis(ethylenedithio)tetrathiafulvalene, this range is confined to the close vicinity of T_c [50], and the experimentally determined $H_{c2}(T)$ curve makes a good experimental example for the shape of the upper critical field in paramagnetically limited superconductors [47]. This dependence is shown in Fig. 7 with the blue line. For all the curves in the figure the slope of lines near T_c was adjusted to match orbital limiting expectations.

In Fig. 7 we plot the data for the 10 and 20 K class samples of $Ba_{1-x}K_xFe_2As_2$ in the $H \parallel a$ configuration in comparison with curves for the orbital and paramagnetic limiting cases. Note that the curve for $x = 0.83$ closely follows expectations for paramagnetic limiting, with a negligible orbital contribution. Interestingly, even the value of the upper critical field for this sample is close to expectations for a weak-coupling superconductor, $H_p = 1.8 \times 10 = 18$ T (see Fig. 6).

The curve for the other overdoped composition, $x = 0.65$, still is very close to expectations for paramagnetic limiting and closely follows experimental data for $CeCoIn_5$ (magenta line), a strongly paramagnetically limited superconductor [51]. The curves for optimally doped samples with $x = 0.39$ (open triangles in Fig. 7) and $x = 0.47$ (solid triangles) are defined in a too narrow range to distinguish clearly between orbital and paramagnetic limits. The data for underdoped compositions with $x = 0.17$ (open circles) and $x = 0.22$ (open squares) are close to orbital limiting. For reference we also plot the literature data for the sample with $x = 1$ [15] and for the underdoped sample with $T_c \approx 28$ K ($x \sim 0.25$) [5]. The curve for the latter sample is very close to the dependence for $x = 0.22$ in our measurements; the curve for $x = 1$ deviates somewhat more from the closest data for $x = 0.83$ in our measurements, revealing a somewhat higher saturation value of H^a_{c2}.

The findings of our study are somewhat unexpected. Paramagnetic effects in $H_{c2}(T)$ are usually found is quite anisotropic materials, like layered organic κ-(BEDT-TTF)$_2$Cu N([CN)$_2$]Br, with $\gamma_\rho \sim 10^3$–10^4. The anisotropy of the resistivity and upper critical fields near T_c in $Ba_{1-x}K_xFe_2As_2$ is significantly lower [9]; in KFe_2As_2, for example, $\gamma_H \sim 5$–7 [9,12,15] and $\gamma_\rho \sim 30$ [24]. This observation might suggest that increased effective masses, as found in heat-capacity [14,46,52,53] and transport [23,29] studies, push orbital upper critical fields up for both in-plane and out-of-plane field orientations, similar to the heavy-fermion materials. In a situation like this, asymmetry of the doping evolution of $H_{c2}{}^a$ may be a reflection of increasing effective mass, as reflected in the increasing electronic heat-capacity coefficient $\gamma_N \equiv C_{el}/T$ on approaching the quantum critical point in the overdoped compositions, rather than electronic anisotropy [46,52]. This would suggest that the H^a_{c2}/T_c ratio should be increased on the overdoped side, which is not the case.

On the other hand, the upper critical field in the $H \parallel ab$ configuration in the underdoped compositions is intermediate between paramagnetic and orbital limiting, despite similar anisotropy values of γ_H and significantly lower normal-state electronic heat capacity γ_N [46]. Notable asymmetry may be related to asymmetry found in the shape of $H^c_{c2}(T)$ with upward deviations from the linear dependence in the underdoped $x = 0.17$ compared to downward deviations in overdoped $x = 0.83$ and $x = 0.65$. In the multiband scenario upward deviation may suggest a notable increase in the effective gap magnitude in $x = 0.17$ on cooling, which can lead to upward deviation even in the paramagnetic limiting regime. It is known that multiband effects are needed to account for heat capacity [46] and London penetration depth [28] for all compositions of $Ba_{1-x}K_xFe_2As_2$. Our observation may be suggestive of stronger multiband effects on the underdoped side.

Another possible source of asymmetry may be coexistence with long-range magnetic order in the compositions $x = 0.17$ and $x = 0.22$ on the underdoped side of the phase diagram but not in $x = 0.65$ and $x = 0.83$ on the overdoped side. Long range magnetic order is known to affect the nodal structure of the superconducting gap, as suggested theoretically [54] and observed experimentally in London penetration-depth [37] and thermal-conductivity [17] measurements. To the best of our knowledge, the effect of the coexisting long range magnetic order on the upper critical field H_{c2} has not been discussed for iron-based superconductors.

V. CONCLUSIONS

By performing a study of the anisotropic upper critical fields in the $Ba_{1-x}K_xFe_2As_2$ series of compounds for a range of compositions spanning from underdoped ($x = 0.17$) to overdoped ($x = 0.83$) in precision-alignment magnetic-field-orientation conditions, we found a strong paramagnetic limiting of H^a_{c2} in the overdoped compositions but not in the underdoped compositions. We speculate that much more pronounced multiband effects on the underdoped side may be responsible for the asymmetry, as suggested by the difference in the shapes of $H^c_{c2}(T)$ dependences.

ACKNOWLEDGMENTS

We thank V. G. Kogan for critical reading of the manuscript and useful discussions. The experimental work was supported by the U.S. Department of Energy (DOE), Office of Basic Energy Sciences, Division of Materials Sciences and Engineering. The experimental research was performed at Ames Laboratory, which is operated for the U.S. DOE by Iowa State University under Contract No. DE-AC02-07CH11358. Work at the National High Magnetic Field Laboratory is supported by NSF Cooperative Agreement No. DMR 1157490 and by the state of Florida.

[1] K. Ishida, Y. Nakai, and H. Hosono, J. Phys. Soc. Jpn. **78**, 062001 (2009).

[2] F. Hunte, J. Jaroszynski, A. Gurevich, D. C. Larbalestier, R. Jin, A. S. Sefat, M. A. McGuire, B. C. Sales, D. K. Christen, and D. Mandrus, Nature (London) **453**, 903 (2008).

[3] N. Ni, S. L. Bud'ko, A. Kreyssig, S. Nandi, G. E. Rustan, A. I. Goldman, S. Gupta, J. D. Corbett, A. Kracher, and P. C. Canfield, Phys. Rev. B **78**, 014507 (2008).

[4] M. M. Altarawneh, K. Collar, C. H. Mielke, N. Ni, S. L. Bud'ko, and P. C. Canfield, Phys. Rev. B **78**, 220505(R) (2008).

[5] H. Q. Yuan, J. Singleton, F. F. Balakirev, S. A. Baily, G. F. Chen, J. L. Luo, and N. L. Wang, Nature (London) **457**, 565 (2009).

[6] J.-L. Zhang, L. Jiao, Y. Chen, and H.-Q. Yuan, Front. Phys. **6**, 463 (2011).

[7] N. R. Werthamer, E. Helfand, and P. C. Hohenberg, Phys. Rev. **147**, 295 (1966).

[8] M. A. Tanatar, N. Ni, C. Martin, R. T. Gordon, H. Kim, V. G. Kogan, G. D. Samolyuk, S. L. Bud'ko, P. C. Canfield, and R. Prozorov, Phys. Rev. B **79**, 094507 (2009).

[9] Yong Liu, M. A. Tanatar, V. G. Kogan, Hyunsoo Kim, T. A. Lograsso, and R. Prozorov, Phys. Rev. B **87**, 134513 (2013).

[10] J. Murphy, M. A. Tanatar, D. Graf, J. S. Brooks, S. L. Bud'ko, P. C. Canfield, V. G. Kogan, and R. Prozorov, Phys. Rev. B **87**, 094505 (2013).

[11] A. M. Clogston, Phys. Rev. Lett. **9**, 266 (1962); B. S. Chandrasekhar, Appl. Phys. Lett. **1**, 7 (1962).

[12] T. Terashima, M. Kimata, H. Satsukawa, A. Harada, K. Hazama, S. Uji, H. Harima, G.-F. Chen, J. L. Luo, and N.-L. Wang, J. Phys. Soc. Jpn. **78**, 063702 (2010).

[13] T. Terashima, K. Kihou, M. Tomita, S. Tsuchiya, N. Kikugawa, S. Ishida, C.-H. Lee, A. Iyo, H. Eisaki, and S. Uji, Phys. Rev. B **87**, 184513 (2013).
[14] S. Zhang, Y. P. Singh, X. Y. Huang, X. J. Chen, M. Dzero, and C. C. Almasan, Phys. Rev. B **92**, 174524 (2015).
[15] D. A. Zocco, K. Grube, F. Eilers, T. Wolf, and H. V. Löhneysen, Phys. Rev. Lett. **111**, 057007 (2013).
[16] S. J. Kuhn, H. Kawano-Furukawa, E. Jellyman, R. Riyat, E. M. Forgan, M. Ono, K. Kihou, C. H. Lee, F. Hardy, P. Adelmann, Th. Wolf, C. Meingast, J. Gavilano, and M. R. Eskildsen, Phys. Rev. B **93**, 104527 (2016).
[17] J.-Ph. Reid, M. A. Tanatar, X. G. Luo, H. Shakeripour, S. R. de Cotret, A. Juneau-Fecteau, J. Chang, B. Shen, H.-H. Wen, H. Kim, R. Prozorov, N. Doiron-Leyraud, and L. Taillefer, Phys. Rev. B **93**, 214519 (2016).
[18] Z. Q. Mao, Y. Maeno, S. NishiZaki, T. Akima, and T. Ishiguro, Phys. Rev. Lett. **84**, 991 (2000).
[19] M. A. Tanatar, T. Ishiguro, H. Tanaka, and H. Kobayashi, Phys. Rev. B **66**, 134503 (2002).
[20] F. Weickert, P. Gegenwart, H. Won, D. Parker, and K. Maki, Phys. Rev. B **74**, 134511 (2006).
[21] Y. Liu, M. A. Tanatar, W. E. Straszheim, B. Jensen, K. W. Dennis, R. W. McCallum, V. G. Kogan, R. Prozorov, and T. A. Lograsso, Phys. Rev. B **89**, 134504 (2014).
[22] H. Fukazawa, Y. Yamada, K. Kondo, T. Saito, Y. Kohori, K. Kuga, Y. Matsumoto, S. Nakatsuji, H. Kito, P. M. Shirage, K. Kihou, N. Takeshita, C.-H. Lee, A. Iyo, and H. Eisaki, J. Phys. Soc. Jpn. **78**, 083712 (2009).
[23] J. K. Dong, S. Y. Zhou, T. Y. Guan, H. Zhang, Y. F. Dai, X. Qiu, X. F. Wang, Y. He, X. H. Chen, and S. Y. Li, Phys. Rev. Lett. **104**, 087005 (2010).
[24] J.-Ph. Reid, M. A. Tanatar, A. Juneau-Fecteau, R. T. Gordon, S. R. de Cotret, N. Doiron-Leyraud, T. Saito, H. Fukazawa, Y. Kohori, K. Kihou, C. H. Lee, A. Iyo, H. Eisaki, R. Prozorov, and L. Taillefer, Phys. Rev. Lett. **109**, 087001 (2012).
[25] K. Okazaki, Y. Ota, Y. Kotani, W. Malaeb, Y. Ishida, T. Shimojima, T. Kiss, S. Watanabe, C.-T. Chen, K. Kihou, C. H. Lee, A. Iyo, H. Eisaki, T. Saito, H. Fukazawa, Y. Kohori, K. Hashimoto, T. Shibauchi, Y. Matsuda, H. Ikeda, H. Miyahara, R. Arita, A. Chainani, and S. Shin, Science **337**, 1314 (2012).
[26] D. Watanabe, T. Yamashita, Y. Kawamoto, S. Kurata, Y. Mizukami, T. Ohta, S. Kasahara, M. Yamashita, T. Saito, H. Fukazawa, Y. Kohori, S. Ishida, K. Kihou, C. H. Lee, A. Iyo, H. Eisaki, A. B. Vorontsov, T. Shibauchi, and Y. Matsuda, Phys. Rev. B **89**, 115112 (2014).
[27] X.-C. Hong, A.-F. Wang, Z. Zhang, J. Pan, L.-P. He, X.-G. Luo, X.-H. Chen, and S.-Y. Li, Chin. Phys. Lett. **32**, 127403 (2015).
[28] K. Cho, M. Konczykowski, S. Teknowijoyo, M. A. Tanatar, Y. Liu, T. A. Lograsso, W. E. Straszheim, V. Mishra, S. Maiti, P. J. Hirschfeld, and R. Prozorov, Sci. Adv. **2**, e1600807 (2016).
[29] V. Taufour, N. Foroozani, M. A. Tanatar, J. Lim, U. Kaluarachchi, S. K. Kim, Y. Liu, T. A. Lograsso, V. G. Kogan, R. Prozorov, S. L. Bud'ko, J. S. Schilling, and P. C. Canfield, Phys. Rev. B **89**, 220509(R) (2014).
[30] F. F. Tafti, A. Juneau-Fecteau, M.-È. Delage, S. R. de Cotrét, J.-P. Reid, A. F. Wang, X.-G. Luo, X. H. Chen, N. Doiron-Leyraud, and L. Taillefer, Nat. Phys. **9**, 349 (2013).
[31] F. F. Tafti, J. P. Clancy, M. Lapointe-Major, C. Collignon, S. Faucher, J. A. Sears, A. Juneau-Fecteau, N. Doiron-Leyraud, A. F. Wang, X.-G. Luo, X. H. Chen, S. Desgreniers, Y.-J. Kim, and L. Taillefer, Phys. Rev. B **89**, 134502 (2014).
[32] T. Terashima, K. Kihou, K. Sugii, N. Kikugawa, T. Matsumoto, S. Ishida, C.-H. Lee, A. Iyo, H. Eisaki, and S. Uji, Phys. Rev. B **89**, 134520 (2014).
[33] M. Rotter, M. Tegel, and D. Johrendt, Phys. Rev. Lett. **101**, 107006 (2008).
[34] E. Hassinger, G. Gredat, F. Valade, S. R. de Cotret, A. Juneau-Fecteau, J.-Ph. Reid, H. Kim, M. A. Tanatar, R. Prozorov, B. Shen, H.-H. Wen, N. Doiron-Leyraud, and L. Taillefer, Phys. Rev. B **86**, 140502(R) (2012).
[35] A. E. Böhmer, F. Hardy, L. Wang, T. Wolf, P. Schweiss, and C. Meingast, Nat. Commun. **6**, 7911 (2015).
[36] J. M. Allred, S. Avci, D. Y. Chung, H. Claus, D. D. Khalyavin, P. Manuel, K. M. Taddei, M. G. Kanatzidis, S. Rosenkranz, R. Osborn, and O. Chmaissem, Phys. Rev. B **92**, 094515 (2015).
[37] H. Kim, M. A. Tanatar, W. E. Straszheim, K. Cho, J. Murphy, N. Spyrison, J.-Ph. Reid, B. Shen, H.-H. Wen, R. M. Fernandes, and R. Prozorov, Phys. Rev. B **90**, 014517 (2014).
[38] J.-P. Castellan, S. Rosenkranz, E. A. Goremychkin, D. Y. Chung, I. S. Todorov, M. G. Kanatzidis, I. Eremin, J. Knolle, A. V. Chubukov, S. Maiti, M. R. Norman, F. Weber, H. Claus, T. Guidi, R. I. Bewley, and R. Osborn, Phys. Rev. Lett. **107**, 177003 (2011).
[39] H. Hodovanets, Y. Liu, A. Jesche, S. Ran, E. D. Mun, T. A. Lograsso, S. L. Bud'ko, and P. C. Canfield, Phys. Rev. B **89**, 224517 (2014).
[40] P. Richard, T. Sato, K. Nakayama, T. Takahashi, and H. Ding, Rep. Progr. Phys. **74**, 124512 (2011).
[41] K. Kihou, T. Saito, S. Ishida, M. Nakajima, Y. Tomioka, H. Fukazawa, Y. Kohori, T. Ito, S.-I. Uchida, A. Iyo, C.-H. Lee, and H. Eisaki, J. Phys. Soc. Jpn. **79**, 124713 (2010).
[42] M. A. Tanatar, N. Ni, S. L. Bud'ko, P. C. Canfield, and R. Prozorov, Supercond. Sci. Technol. **23**, 054002 (2010).
[43] M. A. Tanatar, R. Prozorov, N. Ni, S. L. Bud'ko, and P. C. Canfield, U.S. Patent No. 8,450,246 (1 September 2011).
[44] A. P. Mackenzie, S. R. Julian, G. G. Lonzarich, A. Carrington, S. D. Hughes, R. S. Liu, and D. C. Sinclair, Phys. Rev. Lett. **71**, 1238 (1993).
[45] V. G. Kogan and R. Prozorov, Rep. Progr. Phys. **75**, 114502 (2012).
[46] F. Hardy, A. E. Böhmer, L. de' Medici, M. Capone, G. Giovannetti, R. Eder, L. Wang, M. He, T. Wolf, P. Schweiss, R. Heid, A. Herbig, P. Adelmann, R. A. Fisher, and C. Meingast, Phys. Rev. B **94**, 205113 (2016).
[47] See T. Ishiguro, J. Phys. IV **10**, 139 (2000), for a review of the experimental data.
[48] A. Gurevich, Rep. Progr. Phys. **74**, 124501 (2011).
[49] K. Maki, Phys. Rev. **148**, 362 (1966).
[50] A. E. Kovalev, T. Ishiguro, T. Kondo, and G. Saito, Phys. Rev. B **62**, 103 (2000).
[51] A. Bianchi, R. Movshovich, C. Capan, P. G. Pagliuso, and J. L. Sarrao, Phys. Rev. Lett. **91**, 187004 (2003).
[52] F. Eilers, K. Grube, D. A. Zocco, T. Wolf, M. Merz, P. Schweiss, R. Heid, R. Eder, R. Yu, J.-X. Zhu, Q. Si, T. Shibauchi, and H. v. Löhneysen, Phys. Rev. Lett. **116**, 237003 (2016).
[53] J. S. Kim, G. R. Stewart, Yong Liu, and T. A. Lograsso, Phys. Rev. B **91**, 214506 (2015).
[54] S. Maiti, R. M. Fernandes, and A. V. Chubukov, Phys. Rev. B **85**, 144527 (2012).